

## Supporting Information for

### Quantitative *In Situ* TEM Tensile Fatigue Testing of Nanocrystalline Metallic Ultrathin Films

Ehsan Hosseinian, Olivier N. Pierron\*

#### S1. MEMS Fabrication Process

Fig. S1 shows an overview of the SOIMUMPs fabrication process used for our MEMS devices.<sup>1</sup> Briefly, a n-type silicon-on-insulator (SOI) wafer is first surface doped; see Fig. S1(a). Then a metallic layer is deposited and patterned onto the SOI wafer (Fig. S1(c)), which is followed by the patterning of the Si layer (using a deep reactive ion etching process); see Fig. S1(d). A frontside protective material is applied before the back of the wafer is patterned to provide through-hole structures, an essential aspect of these MEMS devices for in situ TEM purposes; see Fig. S1(e). The frontside protection layer is then removed, as well as the exposed oxide layer from the top surface; see Fig. S1(f).

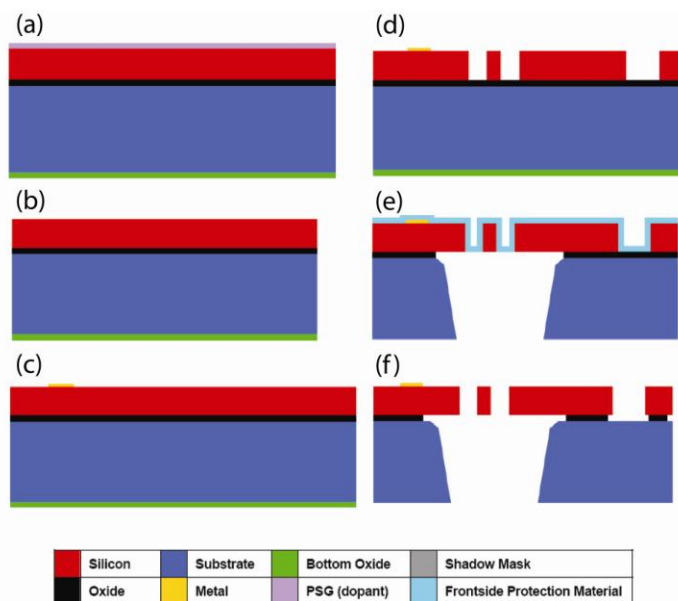


**Fig. S1.** SOIMUMPs fabrication process. See text for details.

## S2. Ultrathin Film Specimen Fabrication Process

Fig. S2 is a schematic of the fabrication process for the ultrathin Au specimens on (100) Si substrates (see Fig. S2(a)). First, photo-lithography (using Karl Suss MA-6 Mask Aligner with 365 nm wavelength) was performed on a 1.5- $\mu\text{m}$  thick negative resist (NR9-1500PY) film that is spin coated on the substrate (see Figs. S2(b) and (c)). After a 20-minute post-baking, the pattern was developed by immersing in a resist developer, RD6. It was then exposed to 90-second descum in a Vision Reactive Ion Etching (RIE) tool to remove any residual resist from the developed areas. High-purity nanocrystalline gold thin films were then deposited using a Denton Ebeam Evaporator at a pressure of  $8 \times 10^{-7}$  Torr and a rate of 0.5  $\text{\AA}/\text{sec}$  (see Fig. S2(d)). The deposition was interrupted after 50 nm for 15 min to minimize the growth of columnar grains.<sup>2</sup> Then, a lift-off technique was used by acoustic agitation in an acetone solution (see Fig. S2(e)). Finally, the specimens were released from the substrate using  $\text{XeF}_2$  as an isotropic etchant of Si (using a Xactix  $\text{XeF}_2$  etcher); see Fig. S2(f). The etch time was chosen so that the specimens were free-standing (due to  $\text{XeF}_2$  partial etching of Si substrate) and connected on one side to a large anchor pad through a small strip for efficient manipulation/placement onto the MEMS device (see Fig. 2).

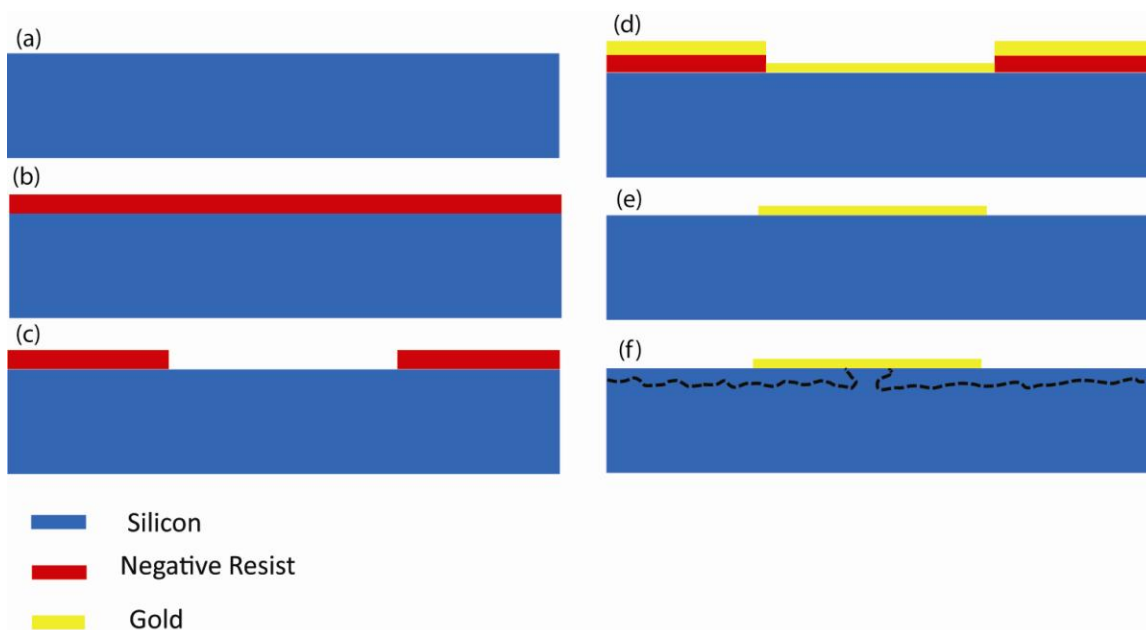


**Fig. S2.** Schematic of the ultrathin gold specimen fabrication process. See text for details.

### S3. MEMS Calibration During *In Situ* TEM Tests

Fig. S3 shows a selection of the bright field TEM images that were used to measure the displacements of the thermal actuator (based on the displacement of the capacitive sensor 1, since  $X_A = X_{CS1}$ ; see Fig. S3(a)) and the load sensor (based on the displacement of the capacitive sensor 2,  $X_{LS}$ ; see Fig. S3(b)) for selected  $V_{in}$  values. The dark areas correspond to the beams of the MEMS device (see Fig. 1(a)), while the bright areas correspond to the gaps between the beams (through-hole MEMS device). The displacements are measured by comparing the images at a given  $V_{in}$  to the reference image at  $V_{in} = 0V$ , using a procedure similar to that described in Ref. [1]. Specifically, the TEM images were overlapped to their reference images ( $V_{in} = 0V$ ), and the relative displacement was measured with an approximate precision of 40 nm for Fig. S3(a) and (b).

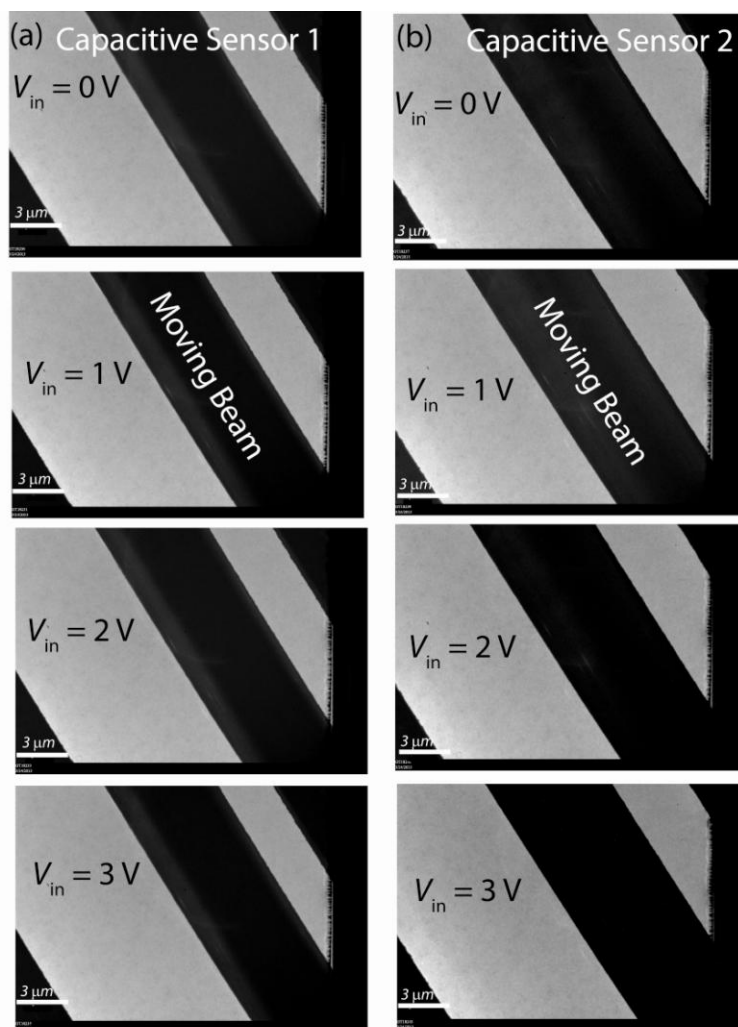


**Fig. S3.** (a) Series of TEM images of capacitive sensor 1 during a fatigue test, at four different  $V_{in}$  values (0, 1, 2, and 3V). (b) Series of TEM images of capacitive sensor 2 during the same fatigue test, at four different  $V_{in}$  values (0, 1, 2, and 3V).

#### **S4. Characterization of MEMS Long-Term Drift**

The long-term stability of the MEMS setup was characterized by monitoring the evolution of the measured capacitance changes for CS<sub>1</sub> (i.e., no specimen attached onto the MEMS device) over large numbers of cycles. Fig. S4(a) shows the typical evolution of the change in measured capacitance at  $V_{in} = 0$  with respect to  $N = 0$ , for more than

6000 cycles. The signal is stable (except for a few cycles between  $N = 500$  and  $N = 1000$  cycles) with a noise of about 0.2 fF. Fig. S4(b) shows the repeatability of the measured  $\Delta C_1$  vs  $V_{in}$  for 100 cycles, also highlighting the precision of these electrical measurements.

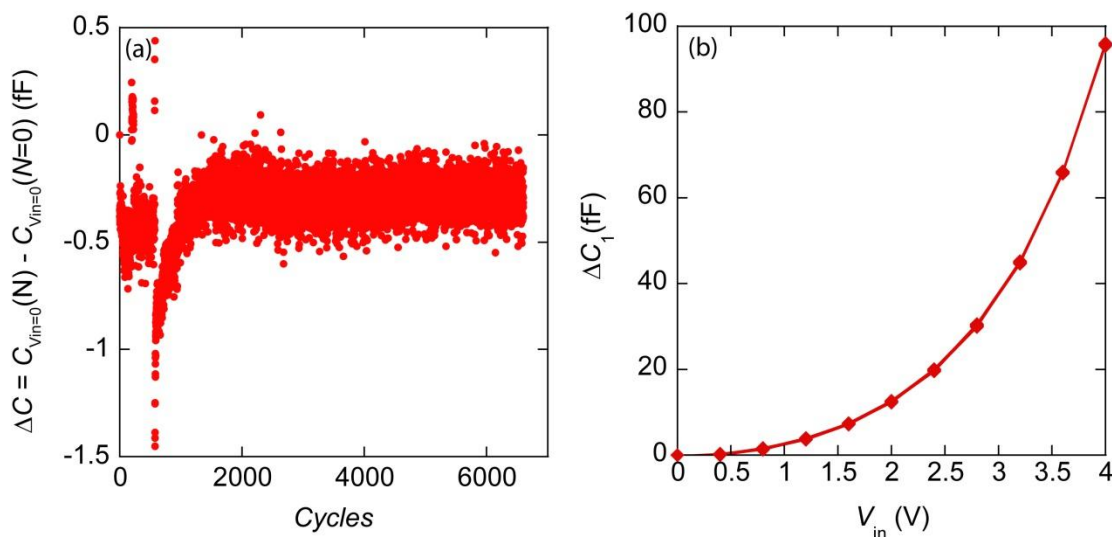


**Fig. S4.** (a) Evolution of capacitance measurement at  $V_{in} = 0V$  for the MEMS setup without a specimen, as a function of cycling (between 0 and 4 V). (b)  $\Delta C_1$  vs  $V_{in}$  measured for 100 consecutive cycles (without a specimen), highlighting the precision and repeatability of the electrical measurements.

### S5. *Ex Situ* Fatigue Test of a Nanocrystalline Ni Nanobeam

A fatigue test was performed on a Ni specimen (length: 14.5  $\mu\text{m}$ , width: 690 nm, thickness:  $\sim 250$  nm) that was manipulated and clamped with ion-beam deposited Pt inside a dual FIB/SEM microscope.<sup>3</sup> The test was performed in laboratory air (*ex situ* test). The applied voltage,  $V_{in}$ , was varied from 0 to 4 V with increments of 0.2 V at a frequency of 0.006 Hz. After 2500 cycles, the test was interrupted for SEM inspection of

the nanobeam. The test was then resumed at a higher frequency of 0.25 Hz. The specimen failed after  $N_f \sim 27,000$  cycles. As explained in the manuscript, the change in capacitance between the two capacitive sensors located on each side of the specimen,  $\Delta C_1 - \Delta C_2$ , was measured as a function of  $V_{in}$ , throughout the test, thereby allowing the monitoring of the specimen's response during cyclic loading. Fig. S5(a) shows four stress-strain curves for selected cycles ( $N = 1, 1000, 2500$ , and  $26,000$ ), while Fig. S5(b)-(d) show the evolution over the first 2500 cycles of the fatigue test of the maximum applied stress,  $\sigma_{max}$ , permanent strain under no applied stress,  $\varepsilon_{\sigma=0}$ , and  $E$ , respectively. Using the unloading portion of the stress strain curve,  $E$  was calculated to increase slightly from 120 to 140 GPa. These values are lower than the  $E$  value for bulk polycrystalline Ni (207 GPa),<sup>4</sup> or the value for <111> out-of-plane textured Ni films (232 GPa),<sup>4</sup> and lower than our previously measured  $E$  value for a similar Ni nanobeam (208 GPa).<sup>5</sup> The low  $E$  values calculated in this experiment are likely the result of compliant Pt clamps. A ratcheting behavior is observed, with the maximum apparent applied strain,  $\varepsilon_{max}$ , increasing from 3.7 to 4.1% throughout the test (see Fig. S5(a)) and a slight decrease in  $\sigma_{max}$  (from 2.8 to 2.6 GPa). Also,  $\varepsilon_{\sigma=0}$  increases from  $\sim 0.3\%$  to 0.7% over the first 2500 cycles. In addition, the decrease in the slope of the stress-strain curve for small strain values (see Fig. S5(a)) is consistent with accumulation of plastic strains: as the specimen is elongated due to plastic deformation, it undergoes buckling near the end of the unloading portion of the cycle, resulting in a lower apparent elastic slope. This result is further confirmed with SEM images of the specimen taken after 2500 cycles (see Fig. S6). It was slightly buckled due to plastic strain accumulation and consequent compressive stress. Fig. S6 also shows SEM images of the specimen after failure ( $N_f = 27,000$  cycles), along with a

high magnification of the fracture surface. The fracture surface occurs away from the Pt clamps and displays an intergranular crack path. In addition, the specimen overlaps by  $\sim 370$  nm at the location of fracture, confirming the accumulation of plastic strains throughout the fatigue test. This value compares well with the calculated plastic overlap (based on the strain value at zero stress prior to fatigue failure) of 250 nm.

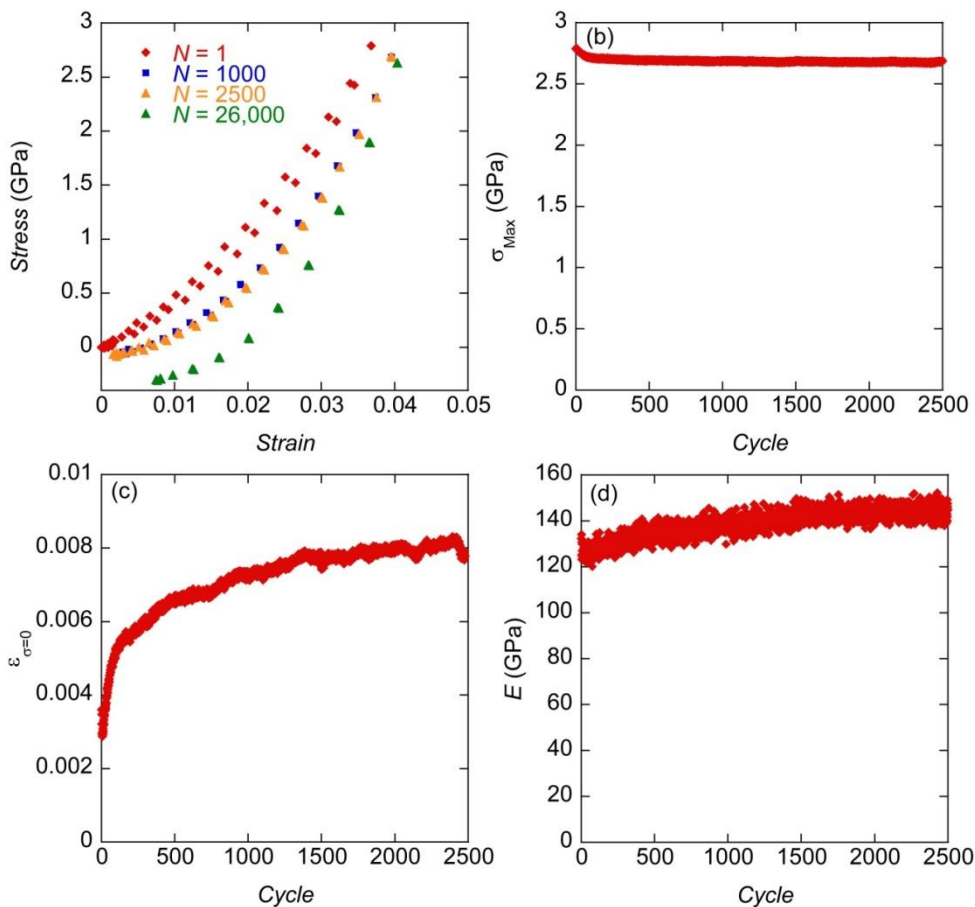


**Fig. S5.** (a) Selected stress-strain curves (for loading and unloading portions of the cycles) at  $N = 1, 1000, 2500,$  and  $26,000$ . (b) Evolution of the maximum applied stress,  $\sigma_{\text{max}}$ , for the first 2500 cycles. (c) Evolution of the permanent strain under no applied stress,  $\epsilon_{\sigma=0}$ , for the first 2500 cycles. (d) Evolution of elastic modulus,  $E$ , for the first 2500 cycles.

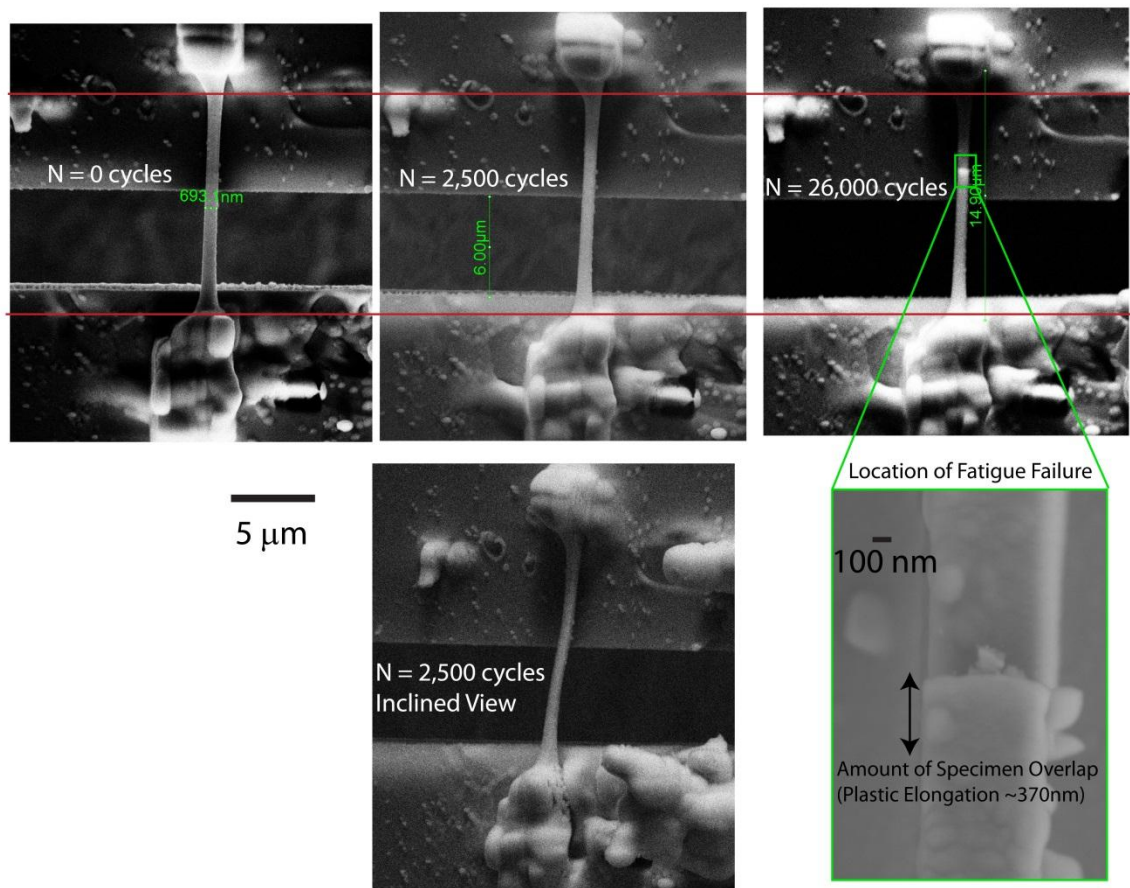


**Fig. S6.** SEM images of the fatigued specimen before test, after 2500 cycles (including inclined view to show buckling effect due to accumulated plastic deformation), and after failure.

In addition to the issue of the compliant Pt clamps, the results of this fatigue test highlight some practical issues associated with the nanobeam manipulation/clamping procedure in the FIB. Specifically, Figure S6 clearly shows the presence of a halo of Pt coatings the entire Ni nanobeam. Also, Ga implantation damage cannot be completely eliminated during the FIB manipulation. This surface damage/modification due to the FIB manipulation can seriously affect the fatigue results and make the interpretation of the

results cumbersome, which motivated the fabrication of the dog-bone shaped specimens that can be manipulated in a “FIB-less” manner (see manuscript).

### **S6 *Ex situ* Monotonic Tests to Failure**

Fig. S7(a) and (b) show the measured  $\Delta C_1 - \Delta C_2$  vs.  $V_{in}$  for two *ex situ* monotonic tests to failure of our Au specimens in laboratory air ( $K_{LS} = 480$  N/m for these experiments). The data are divided into the loading section (from 0 to 4 V for specimen 1 and from 0 to 3 V for specimen 2), and the unloading section (going back to 0 V), along with the same data before the specimen is attached to the MEMS device (representing  $\Delta C_1$  vs.  $V_{in}$ ). Both specimens failed at  $V_{in} = 3$  V, as indicated by the sudden jump in  $\Delta C_1 - \Delta C_2$  value resulting from the second capacitive sensor going back to its original position at the specimen's failure. Once the specimen is failed, the measured  $\Delta C_1 - \Delta C_2$  vs.  $V_{in}$  coincides with the previously measured  $\Delta C_1$  vs.  $V_{in}$  data. The corresponding stress strain curves are shown in Fig. S7(c). The ultimate tensile strengths of the two specimens are 1.3 and 1.2 GPa, for a total strain to failure of 2.5 and 2.3%, and an estimated plastic strain to failure of 0.5 and 0.6%, respectively. The  $E$  values for the two specimens are 54 GPa and 50 GPa respectively, based on a linear fit for strains below 0.2%. As shown below, our measured  $E$  values are larger (70-90 GPa) when using the unloading portion of the stress strain curve (not used for these two monotonic tests to failure), suggesting the possibility of microplasticity during the early part of the loading portion of the stress strain curve.<sup>6</sup> Fig. S7(d) and (e) show SEM images of specimens 1 and 2, respectively, before and after testing, including high magnification images of the fracture surfaces. Both specimens failed along the gauge length, away from the clamps. No obvious apparent deformation of the epoxy clamps could be observed. The fracture surfaces suggest intergranular

failure. The approximate amount of plastic elongation (based on SEM images) was 90 nm for specimen 1, which compares well with the calculated plastic elongation to failure (32 nm using  $E = 54$  GPa, 38 nm using  $E = 70$  GPa). The measured plastic overlap may be larger than the calculated value given that the last calculated stress and strain values are for  $V_{in} = 2.8$  V (for which  $X_{LS} = 529$  nm, corresponding to  $F = 255$   $\mu$ N, and  $X_S = 164$  nm), while the specimen may actually be further deformed at  $V_{in} = 3$  V before it fails. This discrepancy can be minimized by reducing the increments in  $V_{in}$ . In any case, the fact that the calculated plastic elongation (based on the stress strain curve that relies on specimen's crosshead displacement) does not overpredict the measured plastic elongation suggests that the epoxy clamps are stiff and do not deform significantly. Our measured properties are also consistent with previous studies on nanocrystalline Au thin films.<sup>6-11</sup> For example, Yilmaz and Kysar measured  $E = 53$  GPa, a tensile strength of 0.94 GPa, and plastic strain of 2.5% for similar evaporated Au ultrathin films (thickness: 40 nm, width: 350 nm, length: 7  $\mu$ m).<sup>11</sup> Our similar tensile strengths are larger than that measured on specimens with much larger widths or length (hundreds of  $\mu$ m),<sup>6-10</sup> suggesting the possibility of a geometric size effect governing the failure of these nanocrystalline small-scale specimens. Our measured  $E$  values are also consistent with that of other reports that range from 50 to 70 GPa,<sup>6-11</sup> confirming the adequate stiffness of the epoxy clamps.

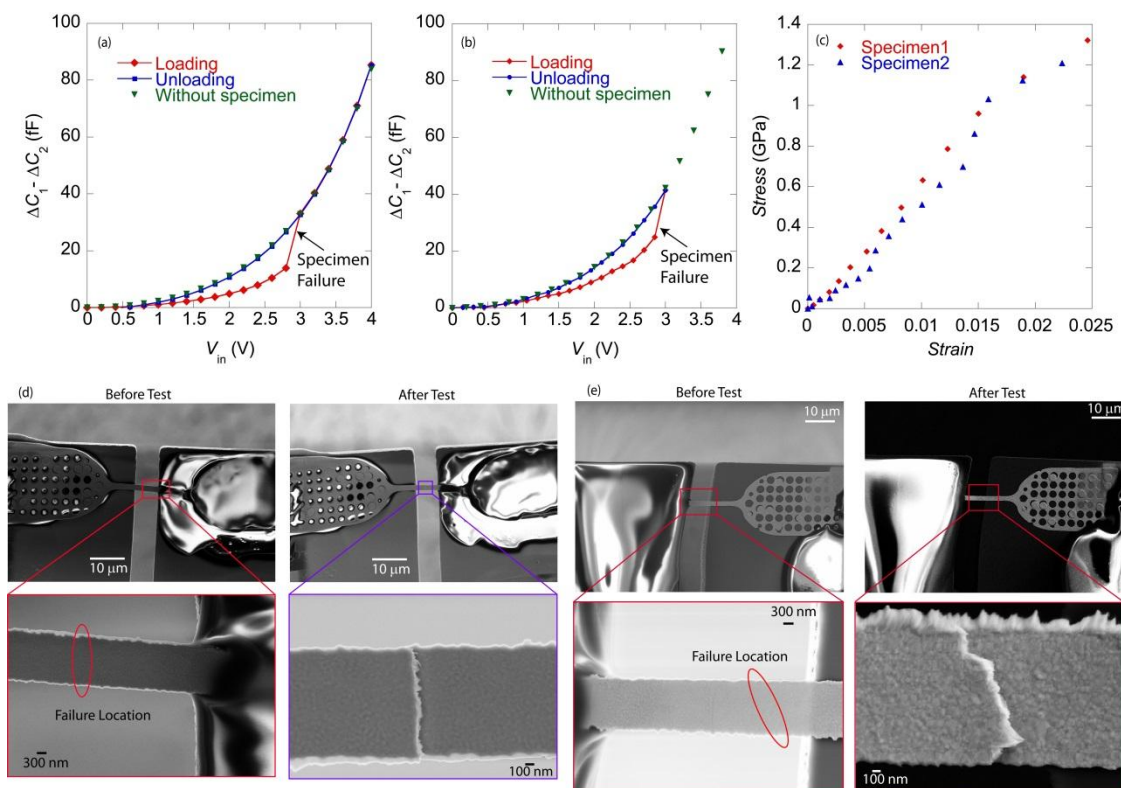


**Fig. S7.** (a) Electrical raw data for monotonic test to failure of specimen 1. (b) Electrical raw data for monotonic test to failure of specimen 2. (c) Corresponding stress-strain curves of specimens 1 and 2. (d) Low and high magnification SEM images of specimen 1 before and after the monotonic test to failure. (e) Low and high magnification SEM images of specimen 2 before and after the monotonic test to failure.

### S7 *In situ* SEM Tests

A series of *in situ* SEM experiments was also performed to observe a MEMS device and the deformed Au specimen during operation, especially at the location of the clamps which cannot be observed inside a TEM. The MEMS device was mounted on a prototype electrical biasing SEM holder (Hummingbird) inside a FEI Nova NanoLab200 dual-beam

microscope. A cyclic test was carried out on one Au specimen before performing a monotonic test to failure. First, cyclic loading was applied by varying  $V_{in}$  between 0 and 2V for approximately 200 cycles. Movies of the deformation of the thermal actuator, both capacitive sensors, and the specimen are shown in Supporting Information (see Movies 1-4). No apparent deformation of the Au specimen's clamps could be observed, confirming the previous results. The specimen was then elongated to failure by increasing  $V_{in}$  from 0 to 4V. Failure occurred along the specimen gauge length, away from the clamps, as shown in Movie 5 in the Supporting Information.

## References

1. <http://www.memscap.com/products/mumps/soimumps>.
2. M. W. Chen, E. Ma, K. J. Hemker, H. W. Sheng, Y. M. Wang and X. M. Cheng, *Science*, 2003, 300, 1275-1277.
3. B. Pant, S. Choi, E. Baumert, B. Allen, S. Graham, K. Gall and O. Pierron, *Exper. Mech.*, 2012, 52, 607-617.
4. K. J. Hemker and H. Last, *Materials Science and Engineering: A*, 2001, 319-321, 882-886.
5. B. Pant, B. L. Allen, T. Zhu, K. Gall and O. N. Pierron, *Appl. Phys. Lett.*, 2011, 98, 053506.
6. J. Rajagopalan, C. Rentenberger, H. P. Karnthaler, G. Dehm and M. T. A. Saif, *Acta Materialia*, 2010, 58, 4772-4782.
7. H. D. Espinosa, B. C. Prorok and B. Peng, *J. Mech. Phys. Sol.*, 2004, 52, 667.

8. M. A. Haque and M. T. A. Saif, *Proceedings of the National Academy of Sciences of the United States of America*, 2004, 101, 6335-6340.
9. K. Jonnalagadda, N. Karanjgaokar, I. Chasiotis, J. Chee and D. Peroulis, *Acta Materialia*, 2010, 58, 4674-4684.
10. J. Rajagopalan, J. H. Han and M. T. A. Saif, *Science*, 2007, 315, 1831-1834.
11. M. Yilmaz and J. W. Kysar, *Nanotechnology*, 2013, 24, 8.